Journal of Applied Fluid Mechanics, Vol. 16, No. 12, pp. 2504-2517, 2023.
Available online at www.jafmonline.net, ISSN 1735-3572, EISSN 1735-3645.
https://doi.org/10.47176/jafm.16.12.1983

Effect of Mesh Shape and Turbulence Model on Aerodynamic Performance at NACA 4415

J. Julian†, W. Iskandar and F. Wahyuni

Department of Mechanical Engineering, Universitas Pembangunan Nasional Veteran Jakarta, 12450, Indonesia

†*Corresponding Author Email: zames@upnvj.ac.id*

ABSTRACT

This study uses three turbulence model variations, i.e., *S - A*, *k - ε*, and *k – ω* turbulence models. In addition, there are two variations of cell shape and three variations of cell number. The number of cells is 500, 5000, 50000, and 100000. Verification is carried out in the mesh refinement study and validated by aerodynamic performances. Based on the mesh refinement study, quadrilateral cells with the *k - ε* are in the asymptotic convergence range. Based on the C_l, it can be concluded that the quadrilateral mesh with 50000 and 100000 cells simulated using the *k-ε* turbulence model shows very low errors, namely 4.1151% and 3.8643%, respectively. It shows consistency based on the quadrilaterals C_d mesh data with the *k-ε* and *k-ω* turbulence models. However, *k-ε* shows the lowest error with the number of cells 50000 and 100000, i.e., 127.7682% and 110.4175%, respectively. However, choosing mesh 50000 cells are advisable because it only takes 23 minutes 48 seconds in computation, while mesh 100000 cells take 1 hour 17 minutes 21 seconds. Only C_m from quadrilateral mesh with the turbulence model *k-ω* shows consistency. An error of mesh 50000 cells is 22.0717%, and the error value for 100000 cells is 18.1630%. By considering computation time, mesh 50000 cells are preferable because it only takes 27 minutes 16 seconds, which is faster 43 minutes 14 seconds than 100000 cells.

Article History

Received May 1, 2023
Revised July 10, 2023
Accepted August 3, 2023
Available online October 8, 2023

Keywords:

Aerodynamic performances
Mesh refinement
Quadrilateral
Triangle
Turbulence models

1. INTRODUCTION

Computational Fluid Dynamics (CFD) is a branch of fluid mechanics that requires a digital computer device to produce predictions of quantitative data from a fluid flow based on the laws of conservation of mass, momentum, and energy as a regulatory equation. The predictions generated by CFD depend on the conditions the user has defined. The conditions in question include boundary conditions, fluid properties, and initial conditions. The output produced by CFD is in the form of variables from fluid flow, including temperature, velocity, vorticity, pressure, density, and others. Furthermore, the predictions generated by CFD can also be in the form of interactions between fluid flow and the body, such as lift force, drag force, moment, and friction (Bhattacharya & Gregory, 2013). CFD can also be called a numerical method. Therefore, the predictions produced by CFD cannot be called exact results. In various research, CFD data is usually used as complementary data from experiments and analytics (Bhattacharya & Ahmed, 2020). The CFD method can produce more detail and comprehensive than the experimental method. In addition, CFD also has other advantages, including parameters that can be changed easily and quickly. For example, the user can adjust the turbulence intensity by changing the input value. CFD can also simulate conditions such as huge or tiny geometric dimensions. Besides simulating actual conditions, the CFD method can also easily simulate ideal conditions such as inviscid fluid flow. With all these advantages, various research related to CFD analysis continues to grow rapidly.

CFD works by using governing equations. The governing equations for viscous fluid movement generally consist of continuity and momentum equations (Jia et al., 2021). However, in the case of turbulent flow, governing equations are paired with the turbulence model. Several turbulence models currently available include the Reynolds Averaged Navier-Stokes (RANS), Large Eddy Simulation (LES), and Direct-Numerical Simulations (DNS). DNS analyzes all turbulence scales in space and time by solving the Navier-Stokes equation. However,

NOMENCLATURE

c	chord length	V	vertices
C_d	drag coefficient	X, Y	coordinates
C_f	friction coefficient	x, y	cartesian coordinates
C_l	lift coefficient	δ	discrepancies
C_m	moment coefficient	ε	dissipation rate
C_p	pressure coefficient	ϵ	relative error of mesh
E	edge	μ	dynamic viscosity of fluids
F	face	ν	kinematic viscosity of fluid
G_k	generation of turbulent kinetic energy due to the mean velocity gradients	ρ	density of fluid
i, j	indices	σ	coefficients in turbulence model
k	turbulent kinetic energy	ω	specific dissipation rate
M	mesh	AoA	angle of attack
p	pressure	CD	central differencing
r	mesh refinement ratio	CFD	Computational fluid dynamics
t	time	GCI	mesh convergence index
U	mean velocity	LUD	linear upwind differencing
u	instantaneous velocity	NACA	national advisory committee for aeronautics
u'	velocity fluctuation	UD	upwind differencing

DNS is very expensive per iteration and only accurate for low-Reynolds Numbers and simple geometries (Zhang et al., 2022). LES resolved a large eddy of turbulent fluid flow. It has a lower cost per iteration than DNS. However, it is still too expensive for practical application (Sirignano et al., 2020). The turbulence model that is currently very reliable in simulating turbulent fluid flow is RANS. RANS can model all turbulent length scales. In addition, the cost per iteration is also lower. RANS consists of several models, namely Spalart-Allmaras (S-A), which consists of one equation. Besides, the RANS model can also be found in two equations such as k-ε and k -ω (Hornshøj-Møller et al., 2021).

Besides being influenced by the governing equations and turbulence models, CFD accuracy is also heavily influenced by meshing. Meshing is a process of converting a continuous domain into a discrete domain to solve an equation numerically. The more discrete domains resulting from the meshing process, the greater the computational burden. A large computational load causes the computational process to take longer, making it inefficient in terms of time. Therefore, the number of discrete domains must be seriously considered (Ali et al., 2017).

A study by Ahadi et al. (2018) discusses the standard turbulence model under flow separation conditions. The standard turbulence models discussed are S - A and k - ε. Besides that, the LES and E-LES turbulence models are also used. The results obtained then compared visually with experimental data. The object used is NACA 0025, simulated on various Reynolds numbers. The LES and E-LES turbulence models show consistent results with the experimental data but only at low Reynolds numbers. However, the S - A turbulence model gives the best results. Aftab et al. (2016) examine the flow modeling around NACA 4415. The turbulence models used are S - A, Menter k - ω, Intermittency (γ), SST k - ω, k - kl - ω, and γ-$Re\boldsymbol{\theta}$ SST. The computational process is performed on the Reynolds number 120000. The mesh used is a structured mesh with quadrilateral cells. The computational results validated with experimental results but only at an Angle of Attack (AoA) of 6° and 18°. Validation is done by comparing the values of C_l, C_d, C_p, boundary layer plots, and C_f. There are several conclusions; First, the S – A model is performing well and can provide excellent initial predictions at low Reynolds numbers from the point of view of aerodynamic forces. Second, the SST k - ω turbulence and Intermittency γ SST models showed identical results. Both can show the formation of a separation bubble; however, they cannot display it in a clear form. So, it can be concluded that the two turbulence models are unsuitable for low Reynolds numbers. Third, the k - kl - ω turbulence model shows promising results at AoA=6°; however, this model requires quite a lot of computational time. The C_p curve also shows results following the experimental results. On the other hand, this model is less reliable to get the value of C_f. Fourth, the γ-$Re\boldsymbol{\theta}$ SST turbulence model shows the best results than other turbulence models in the study. Suvanjumrat (2017) uses open-source code software to compare turbulence models with fluid flow objects in NACA 0015. The turbulence models compared are S - A, k - ω, and SST k - ω. The Reynolds numbers selected are 1.5×10^5 and 3.6×10^5 with the AoA from 0° to 20°. The selected mesh is an unstructured mesh type with triangle cells. The schemes compared are central differencing (CD), upwind differencing (UD), and linear upwind differencing (LUD). The computational results compared to the experimental data by calculating the average error of each turbulence model. The conclusion is that the most suitable turbulence model is k – ω SST. If combined with the scheme, the SST k - ω turbulence model with the LUD scheme is the most suitable.

All studies are summarized in Table 1. Some studies have directly compared turbulence models, but most of those studies only compared modified turbulence models of k – ε and k – ω. So far, no study has directly compared the standard k – ε and k – ω turbulence models, so this

Table 1 10 studies that discussed the turbulence model and mesh

Study	Turbulence models												Meshing category			
	S - A	*k - ε*	*k - ω*	*k – ε* Realize-able	RNG *k - ε*	*k-kl-ω*	SST *k - ω*	RSM	LES	E-LES	γ SST	γ-Reθ SST	Stru-ctured mesh	Unstruc-tured mesh	Quadri-lateral	Tri-angle
Villalpando et al. (2011)	✓	×	×	×	✓	×	✓	✓	×	×	×	×	✓	×	✓	×
Khan et al. (2020)	×	×	×	×	×	✓	✓	×	×	×	×	×	✓	×	✓	×
Sadikin et al. (2018)	✓	×	×	✓	×	×	×	✓	×	×	×	×	✓	×	✓	×
Kumar (2019)	✓	×	×	✓	×	×	✓	✓	×	×	×	×	✓	×	✓	×
Ahadi et al. (2018)	✓	✓	×	×	×	×	×	×	✓	✓	×	×	✓	×	✓	×
Hills et al. (2005)	✓	×	×	✓	×	×	✓	✓	×	×	×	×	✓	×	✓	×
Kekina and Suvanjumrat (2017)	✓	×	×	×	✓	×	✓	×	×	×	×	×	×	✓	×	✓
Suvanjumrat (2017)	✓	×	✓	×	×	×	✓	×	×	×	×	×	×	✓	×	✓
Islam et al. (2016)	×	×	×	×	×	✓	✓	×	×	×	×	×	✓	×	✓	×
Aftab et al. (2016)	✓	×	×	×	×	✓	✓	✓	×	×	✓	✓	✓	×	✓	×
Current study	✓	✓	✓	×	×	×	×	×	×	×	×	×	✓	×	✓	✓

study attempts to fill this gap to provide a more comprehensive understanding of the turbulence model. In addition, studies that discuss the comparative turbulence model from the S-A turbulence model to the $k-\varepsilon$ and $k-\omega$ under the same fluid flow conditions have not yet been carried out, so this is also the aim of this study. This study further discusses the influence of cell shape and turbulence models on the structured mesh. The results of this study also open a discussion regarding the effect of the accuracy of each turbulence model on changes in the number of mesh cells. The discussion in this study will provide an overview of a good combination of turbulence models and two-dimensional cell meshing types.

2. METHODOLOGY

2.1 Standard *S-A*

S-A is a turbulence model based on the eddy viscosity transport equation. This equation can be defined mathematically in equation 1. The *S-A* turbulence model has developed to be applied to aerodynamic flows. In particular, this model is applied to transonic and supersonic flows on airfoils or boundary-layer flows such as adverse pressure gradients. *S-A* is not good enough to model three-dimensional fluid flows. However, the main advantage of this model is that the cost per iteration is very low compared to the two-equation models that will be discussed next (Panagiotou et al., 2015).

$$\frac{D\tilde{v}}{Dt}=G_v\left\{\frac{\partial}{\partial x_j}\left[\left(\mu+p\tilde{v}\right)\frac{\partial\tilde{v}}{\partial x_j}\right]+C_{b2\rho}\left(\frac{\partial\tilde{v}}{\partial x_j}\right)^2\right\} -Y_v+S_{\tilde{v}} \quad (1)$$

Where $\tilde{v}$ defines modified eddy viscosity, t time, x_j cartesian coordinate, μ the dynamic viscosity, p for pressure, $C_{b2\rho}$ clossure constant, G_v, Y_v, and $S_{\tilde{v}}$ are diffusive terms .

2.2 Standard *k - ε*

The standard $k-\varepsilon$ turbulence model is developed by Launder and Spalding. This turbulence model is the most popular among the other two-equation turbulence models. Standard $k-\varepsilon$ is a suitable model for simulating internal or external flow and handling various fluid flow conditions. In addition, it is also suitable for the initial screening of alternative designs, initial iterations, and parametric studies (Julian et al., 2022a). However, this model is unsatisfactory for complex fluid flows such as severe pressure gradient and strong streamlined curvature. The $k-\varepsilon$ turbulence model is based on the transport equation for turbulent kinetic energy k and dissipation rate ε (Julian et al., 2023a). The equations for the $k-\varepsilon$ turbulence model are defined in equations 2 and 3 (Launder & Spalding, 1983).

$$\frac{D}{Dt}(\rho k)=\frac{\partial}{\partial x_j}\left[\left(\mu+\frac{\mu_t}{\sigma_k}\right)\frac{\partial k}{\partial x_j}\right]+G_k-\rho\varepsilon \quad (2)$$

$$\frac{D}{Dt}(\rho\varepsilon)=\frac{\partial}{\partial x_j}\left[\left(\mu+\frac{\mu_t}{\sigma_\varepsilon}\right)\frac{\partial \varepsilon}{\partial x_j}\right]+C_{e1}\frac{\varepsilon}{k}G_k -\rho C_{\varepsilon 2}\frac{\varepsilon^2}{k} \quad (3)$$

where ρ is density, ε turbulent dissipation energy, k turbulent kinetic energy, $C_\mu=0.09$, $C_{\varepsilon 1}=1.44$, $C_{\varepsilon 2}=1.92$, $\sigma_\varepsilon=1.3$

2.3 Standard *k* - *ω*

Standard *k* - *ω* is the two equations turbulence model developed by Wilcox (1998), which is specially formulated to calculate the effects of low Reynold number, shear flow spreading, and compressibility. This turbulence model is based on the transport equation for kinetic energy *k* and its specific dissipation rate *ω* (Julian et al., 2022b). Furthermore, this model accurately simulates a boundary layer with a pressure gradient. Mathematical model of standard *k* - *ω* is given in equation 4 and equation 5 (Wilcox, 1998).

$$\rho\frac{Dk}{Dt}=\tau_{ij}\frac{\partial\overline{u_i}}{\partial x_j}-\rho\theta f_{\beta^*}k\omega+\frac{\partial}{\partial x_j}\left[\left(\mu+\frac{\mu_t}{\sigma_k}\right)\frac{\partial k}{\partial x_j}\right] \quad (2)$$

$$\rho\frac{D\omega}{Dt}=\alpha\frac{\omega}{k}\tau_{ij}\frac{\partial\overline{u_i}}{\partial x_j}-\rho\beta f_\beta\omega^2+\frac{\partial}{\partial x_j}\left[\left(\mu+\frac{\mu_t}{\sigma_\omega}\right)\frac{\partial\omega}{\partial x_j}\right] \quad (3)$$

where $\omega=\frac{\varepsilon}{k}\propto\frac{1}{\tau}$, $\mu_t=\alpha^*\rho\frac{k}{\omega}$, and $\overline{u_i}$ mean *x* velocity, τ_{ij} shear stress

2.4 Meshing

The mesh is two-dimensional and structured (Julian et al., 2023b). The structured mesh is relatively easier to make tight as it approaches the airfoil than the unstructured mesh. It needs to be done because several phenomena often appear around the surface of the airfoil, so it is necessary to have a tight mesh around the surface to get accurate results. The form of cells or meshing cells in this computational process consists of two types, namely quadrilaterals, and triangles. The advantage of quadrilateral cells is that they produce better mesh quality with fewer cells than triangle cells. On the other hand, because mesh triangles are often used on unstructured mesh, it will produce a mesh with a relatively shorter time. A cell mesh (*M*) generally consists of several components, i.e., vertices (*V*), edge (*E*), and Face (*F*), or can be written as *M* = {*V*, *E*, *F*}. Each component is defined as *V*

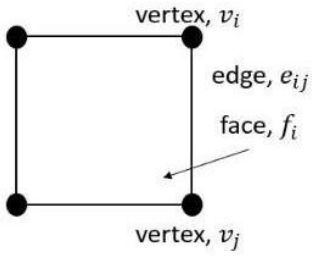

(a) Quadrilateral cell

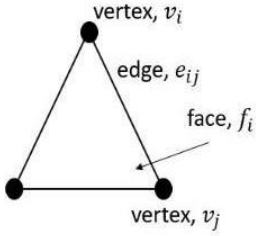

(b) Triangle cell

Fig. 1 Two-dimensional cell shape

$=\{v\}_{i=1}^{Nv}$, $E=\{e\}_{i=1}^{Ne}$ $F=\{f\}_{i=1}^{Nf}$. Edges connect vertices. For example, an edge eij connecting vertices vi and vj. Meanwhile, a bunch of multiple edges will produce a polygon face. The faces are the same as cells in a two-dimensional mesh, but this does not apply to a three-dimensional mesh. A cell with three edges will produce a triangle cell, whereas if a cell has four edges, it will produce a quadrilateral cell (Bouaziz et al., 2012). An overview of the explanation above can be seen in Fig. 1.

2.5 NACA 4415

NACA 4415 is one of the NACA four series. Most airfoils should be made with a minimum of 50 points on the surface. The camber of four-digit NACA can be made from equation 7, which consists of two parabolic equations corresponding to the maximum camber point (Julian et al., 2022c). The 4-digit number of NACA 4415 means the thickness ratio is 15%, with the maximum camber located at x=40% of the chord(c). NACA 4415 is chosen because it has a unique feature. This type of airfoil can generate excellent lift forces even in unstable fluid flows so that the data in this study can be utilized in a wider range of areas. Therefore, NACA 4415 airfoil is generally used as wind turbine blades and can be used as a UAV. The NACA 4415 is depicted in Fig. 2.

2.6 Fluid flow domain

The domain used during the computational process consists of semicircles and rectangles. The diameter of the semicircle is fixed with the width of the rectangle. As shown in Fig. 3, the length of the side BC is 20c. c is defined as airfoil chord(Anzalotta et al., 2020). The tail of the airfoil is located right in the center of the semicircle(Julian et al. 2022d). Domain sizes are arranged to minimize the effect of the boundary locations.

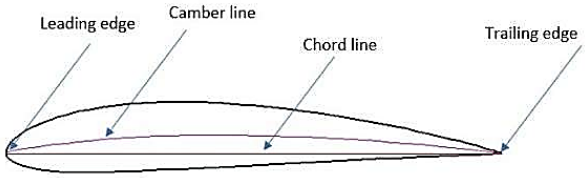

Fig. 2 NACA 4415

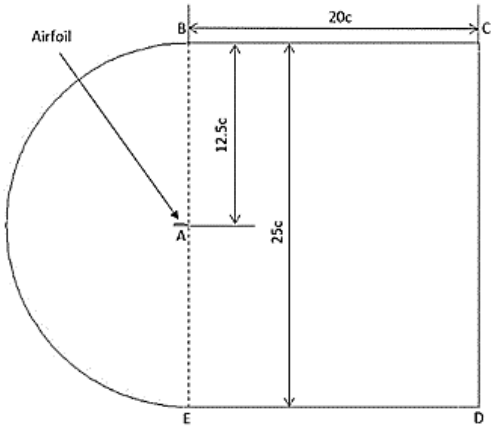

Fig. 3 Domain used in the computational Process

2.7 Computation Setup

Boundary conditions in the computational process consist of velocity inlet and pressure outlet. The position of the boundary condition follows the research conducted by Iskandar et al., 2022. The Reynolds number used is 10^6. While the algorithm used is pressure-based SIMPLE (Joshi & Bhattacharya, 2019). Meanwhile, the outlet pressure is 0. The mesh used in the computational process consists of three variations in the number of cells. The first is the finest mesh with 50000 cells; the second variation is a mesh with 5000 cells; the third mesh variation is 500. The mesh with quadrilateral cells can be seen in Fig. 4, while the mesh with the cell triangle type can be seen in Fig. 5. The quality of the mesh in each mesh variation is maintained by applying the value $y^+<1$. It aims to ensure the mesh is in the viscous sub-layer area ($y^+\leq5$) to obtain satisfactory computational results. In addition, at $y^+\leq5$, it can predict the fluid flow features near the wall very well (Reggio et al., 2011). The distribution of y^+ values along the airfoil surface is given in Fig. 6.

3. Results and Discussion

3.1 Mesh Refinement Study

The mesh refinement study in this paper uses fluid velocity as a test variable. Data is taken at coordinates x=0.8 and y=0.1 with AoA=0°. Each process of the mesh independence test is carried out as in the research Iskandar et al (2022). Based on the results obtained from the mesh refinement study, the *k-ε* turbulence model with quadrilateral cells is in the asymptotic convergence range,

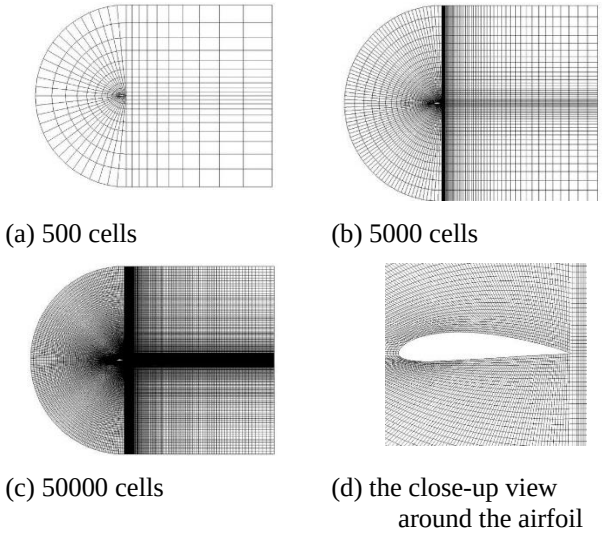

(a) 500 cells (b) 5000 cells

(c) 50000 cells (d) the close-up view around the airfoil

Fig. 4 Quadrilaterals mesh used in this study

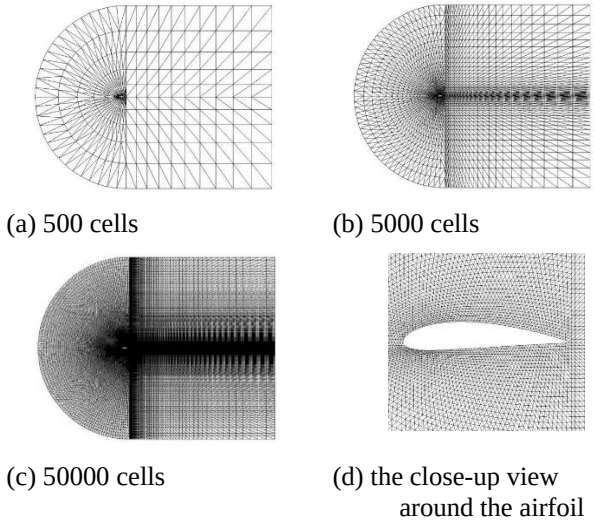

(a) 500 cells (b) 5000 cells

(c) 50000 cells (d) the close-up view around the airfoil

Fig. 5 Triangles mesh used in this study

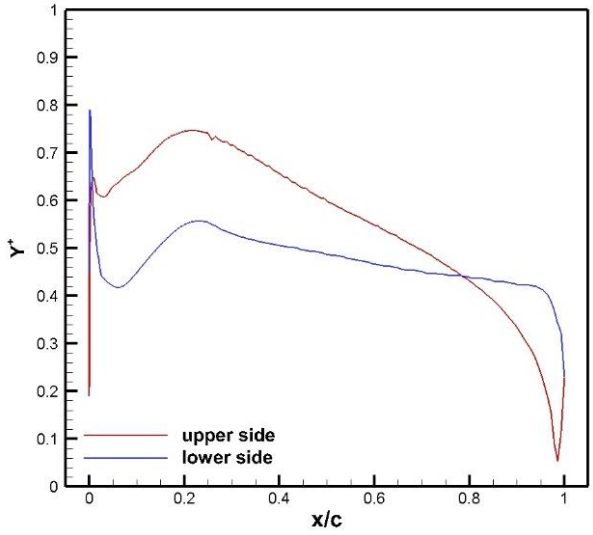

Fig. 6 y^+ distribution along the airfoil

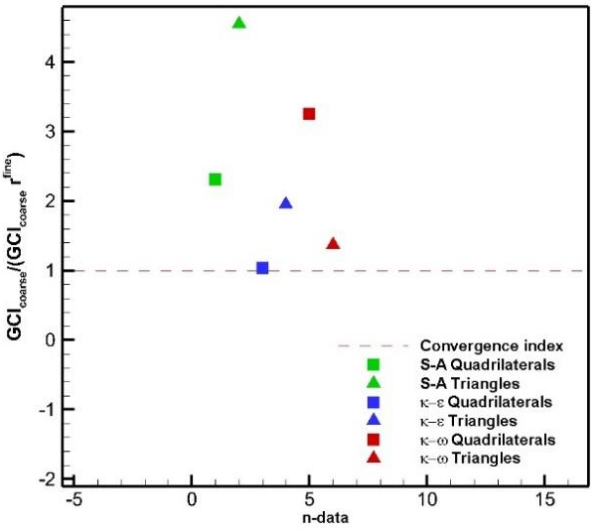

Fig. 7 Results of verification

which is indicated by a number close to 1(Julian et al., 2023c). Overall, the mesh refinement study results can be seen in Table 2 and Fig. 7.

In this paper, the aerodynamic performance will be used as a reference to validate the computational results. Validation is done by comparing the data obtained from the computational process with experimental results and then calculating the average error value against the experimental results used as a reference.

The experimental studies featured are Jacobs and Sherman (1937), Loftin and Smith (1948), and Hoffmann et al. (1996). However, the data used as a reference for calculating the average error value is the study of Hoffmann et al. (1996). This study is chosen because it has complete data and is the most recent study among others. The experimental studies of Loftin and Smith (1949) and Hoffmann et al. (1996) are carried out on the Reynolds number 10^6, while the study conducted by Jacobs and Sherman (1937) is carried out by applying the Reynolds number of 1.3×10^6. The study of Jacobs and Sherman (1937) can be used because the Reynolds number used is still in the moderate Reynolds number regime, and the Reynolds number difference is relatively not too far away. Apart from using experimental data, this research also includes computational studies from research conducted by Siddiqi and Lee (2019) on the same Reynolds number, i.e., 10^6.

3.2 Results of computation

Figure 8(a) shows the C_l data of the S - A turbulence model with quadrilateral cells. Mesh with 5000 and 50000 cells show results close to the experimental data. However, both predict stall conditions faster than experimental data. Meanwhile, the mesh with 500 cells shows poor results compared to the experimental data. Even the mesh cannot predict stall conditions. If the number of cells is increased to 100000, the resulting data accuracy is no better when compared to a mesh of 50000 cells.

It is supported It is supported by the fact that the stall occurs two degrees faster. A much different result can be seen in Fig. 8(b), which is C_l for a mesh with triangle cells and the *S-A* turbulence model. Things are very different with the triangle mesh. As shown in Fig. 8(b), it can be seen that the mesh that gives the best results is the mesh with 5000 cells. When the number of cells is increased to 50000 and 100000 cells, the accuracy obtained decreases drastically. The results show a very different trend if the number of cells used is 500. Better results are shown by the combination of the k - ε turbulence model with 50000 quadrilateral cells in Fig. 8(c). In addition to showing results close to experimental data, this combination also predicts AoA stall very well. Meanwhile, for the mesh with 5000 cells and 500 quadrilaterals for the k - ε turbulence model, the results are not much different from the S - A turbulence model.

Table 2 Mesh refinement study results

Turbulence model	Cells	Mesh normalized	Mesh Spacing	Velocity	p	Results	$V_{rh=0}$
S-A	Quadrilateral	1	500	15.6305	24.1183	2.3090	15.6340
		2	5000	15.5778			
		3	50000	14.7311			
	Triangle	1	500	14.3402	14.2659	4.5426	14.2659
		2	5000	15.1846			
		3	50000	15.348			
k-ε	Quadrilateral	1	500	16.4742	34.0770	1.0381	16.4744
		2	5000	16.4604			
		3	50000	15.7626			
	Triangle	1	500	15.9836	26.2717	1.9437	15.3344
		2	5000	15.366			
		3	50000	15.336			
k-ω	Quadrilateral	1	500	15.5879	19.3382	3.2525	15.5969
		2	5000	15.5132			
		3	50000	14.821			
	Triangle	1	500	17.0169	30.6885	1.3680	15.3419
		2	5000	15.3909			
		3	50000	15.3434			

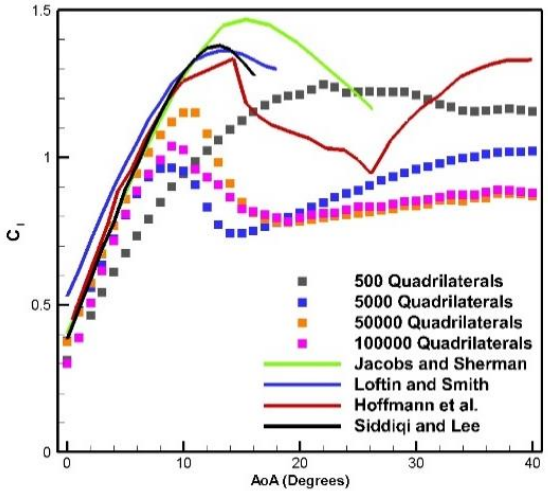

(a) S – A quadrilaterals

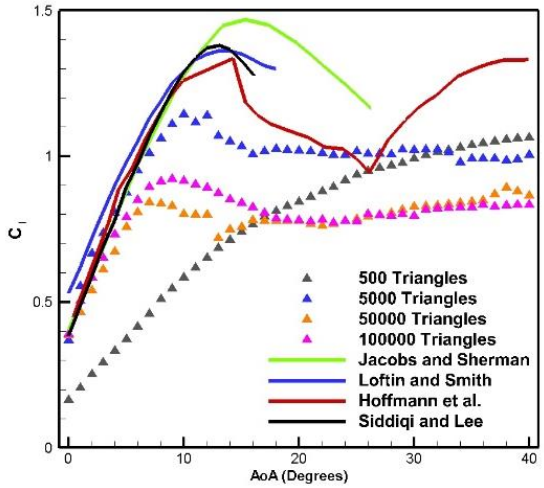

(b) S – A triangles

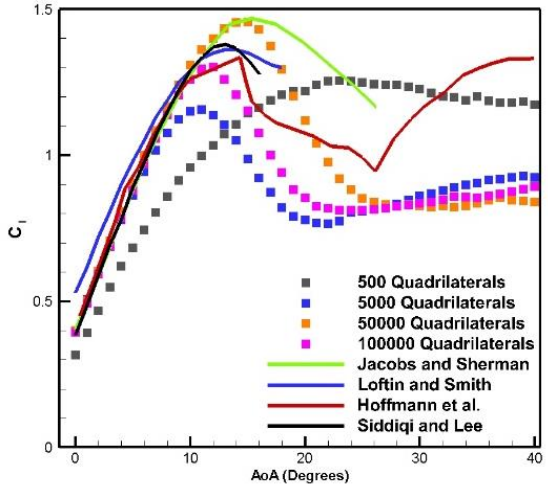

(c) k - ε quadrilaterals

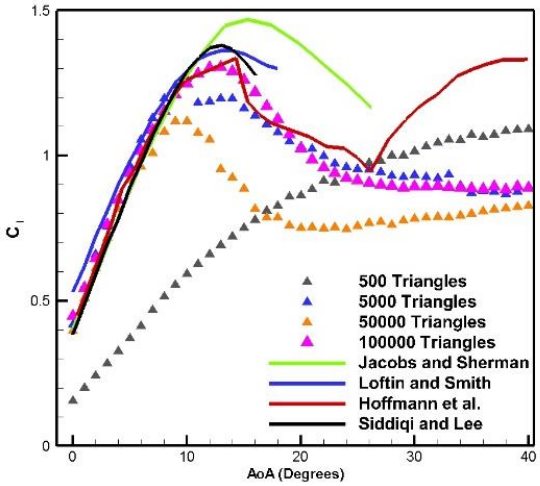

(d) k - ε triangles

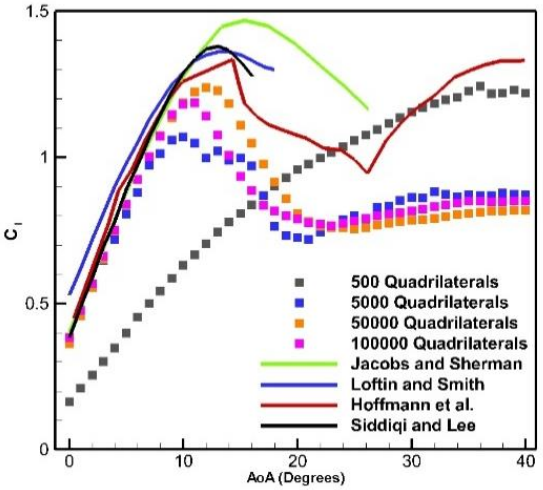

(e) $k-\omega$ quadrilaterals

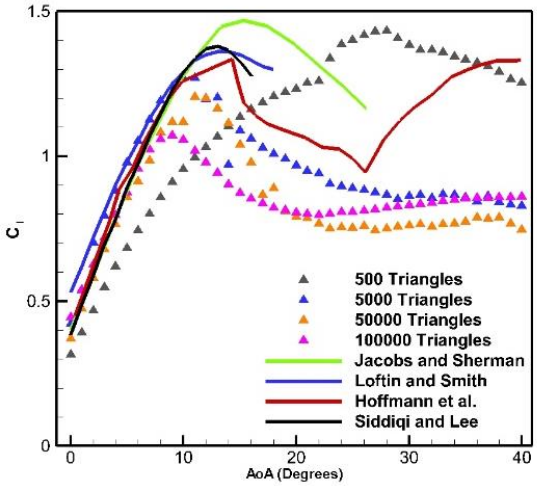

(f) $k-\omega$ triangles

Fig. 8 Plot C_l vs. AoA of each turbulence model and cell shape

If the number of cells increases, the results will be even better, especially in the AoA before a stall occurs. However, the stall becomes 1° faster. Figure 8(d) also shows the computational results for the k – ε turbulence model but with triangle cells. This combination can handle triangle cells with all the number of cells tested. The mesh with 5000 and 50000 cells predicts stalls at the same AoA but faster than the experimental results. Like the others, for the 500 triangle cells, the k – ε model also shows not good results. Accuracy will be better when the number of cells is increased to 100000. It shows an inconsistency if the k–ε turbulence model uses a triangle cell. Furthermore, Fig. 8(e) shows the computational results for the k - ω turbulence model with quadrilateral cells. Note that the results obtained for the combination different from the k-ε turbulence model with the same k–ω and quadrilaterals

Table 3 Average error percentages of all combinations of turbulence model and cell shape in predicting C_l

Turbulence model	Cells	Number of cells	Average error percentages	
			0°≤AoA≤14°	15°≤AoA≤40°
S-A	Quadrilateral	500	24.6837%	12.3103%
		5000	20.5589%	20.7184%
		50000	11.3797%	27.5601%
		100000	20.5220%	26.1249%
	Triangle	500	55.8844%	17.8371%
		5000	9.2152%	12.2665%
		50000	22.6047%	13.0297%
		100000	19.4000%	29.1418%
k-ε	Quadrilateral	500	23.7713%	12.4707%
		5000	8.4721%	25.0829%
		50000	4.1151%	22.9626%
		100000	3.8643%	23.1600%
	Triangle	500	56.0460%	16.0626%
		5000	4.5072%	15.1200%
		50000	9.7219%	31.2272%
		100000	1.8717%	16.3584%
k-ω	Quadrilateral	500	23.8734%	16.7128%
		5000	14.9408%	27.0128%
		50000	8.7002%	27.7736%
		100000	10.1886%	27.8048%
	Triangle	500	53.1473%	8.8366%
		5000	6.2261%	20.2206%
		50000	9.1078%	30.3611%
		100000	11.7389%	26.8369%

cells are not much cell type. However, there is a difference where the stall is predicted to be several degrees faster than the experimental results. On the other hand, in triangle cells, the best data is also shown by a mesh with 5000 cells, as shown in Fig. 8(f).

After determining the best turbulence model and the best cell shape, the next step is to determine the number of cells to be selected. The mesh chosen is the mesh that gives the smallest average error value. Based on all the considerations in Table 3. The AoA that is the primary consideration is in the range 0°≤AoA≤14°. Because the airfoil has not experienced a stall, the fluid flow conditions have not become chaotic due to circulating flow. In the S-A turbulence model, it can be seen that the combination that produces the lowest error is the triangle mesh with the number of cells 50000, where the resulting error is 9.2152%. In the *k–ε* turbulence model, the combination that produces the smallest error is the quadrilateral mesh with 100000 cells with an average error of 3.8643%. However, if the mesh is reduced to 50000, the resulting error is not much different, namely 4.1151% and only takes 23 minutes 48 seconds. This is faster than mesh 100000 cells which need 1 hour 17 minutes and 21 seconds. If using the k–ω turbulence model, the combination that gives the smallest error is a triangle mesh with a total of 5000 cells. However, if required to use the *k–ω* turbulence model with quadrilateral cells, the most recommended number of cells is 500000.

Figure 9(a) shows the drag coefficient for the S - A turbulence model with quadrilateral cells. As the number of cells increases, the computational process's accuracy will improve. It is proven by the identical results obtained between mesh with 50000 cells and experimental data. This pattern is also seen when the number of cells is increased again to 100000, where the resulting data is closer to the experimental data. Figure 9(b) shows the computational results with the *S - A* turbulence model in triangle cells. Based on observations, a mesh with 5000 cells shows the best results. However, this only applies to low AoA. When AoA is increased, the mesh that gives the lowest value is the mesh with a total of 100000 cells. Figure 9(c) discusses the computational results for the *k - ε* turbulence model with quadrilateral cells. Like the S - A turbulence model, the mesh that gives the best results for this combination is a mesh with 50000 cells. If further observed, a mesh with a cell number of 5000, 50000, and 100000 cells show similar results at low AoA. Figure 9(d) is the computational result for the same turbulence model, i.e., *k - ε*, but with the shape of cell triangles. Mesh with 500 cells shows a slight difference at low AoA. However, a mesh with 500, 5000, and 100000 cells shows results quite close to each other when the AoA airfoil is extreme. Figure 9(e) is the computational result of the *k - ω* turbulence model for quadrilateral cells, while Fig. 9(f) is the computational result for triangle cells. The two images show that the mesh with triangle cells is more precise than quadrilateral cells in predicting C_d. A more detailed and in-depth explanation will be discussed by comparing the error values of each number of cells.

The percentage error calculation for C_d slightly differs from C_l because the experimental data for C_d used as a reference is very limited. Therefore, the percent error calculation is only in one interval, 0°≤AoA≤9°. The first consideration is the consistency of the mesh. Quadrilateral cells with $k - \varepsilon$ and $k - \omega$ show consistency.

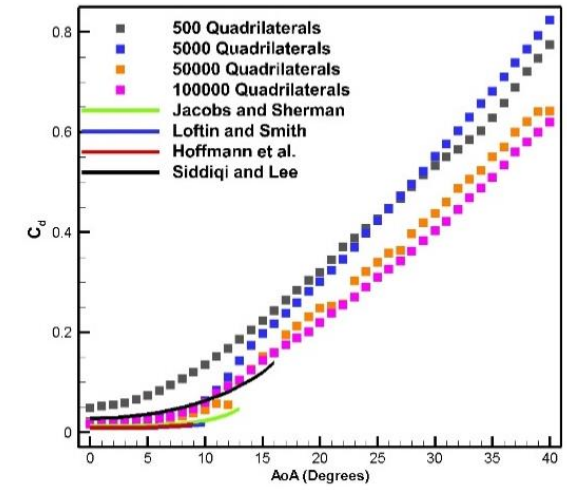

(a) S – A quadrilaterals

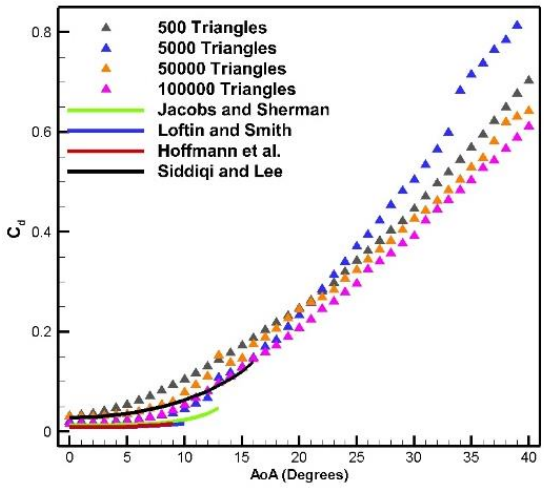

(b) S – A triangles

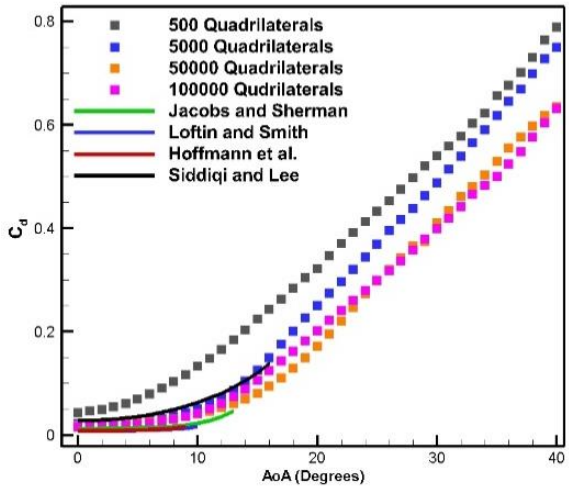

(c) k - ε quadrilaterals

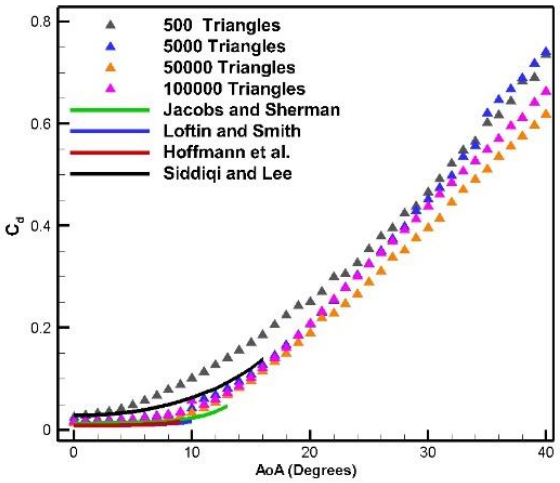

(d) k - ε triangles

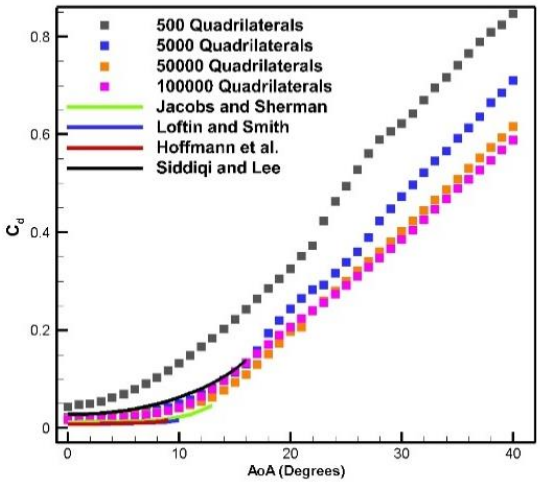

(e) $k-\omega$ quadrilaterals

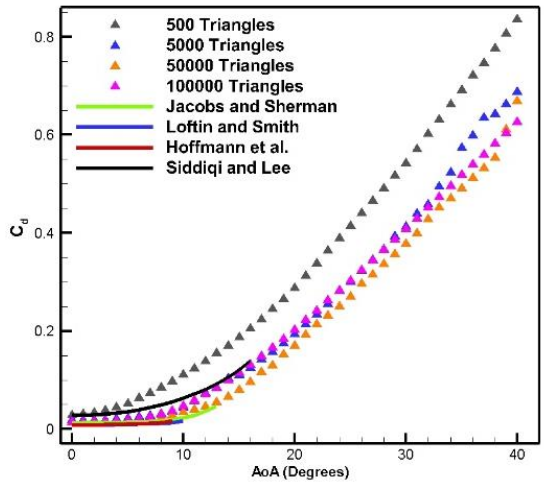

(f) $k-\omega$ triangles

Fig. 9 Plot C_d vs. AoA of each turbulence model and cell shape

However, *the* $k-\varepsilon$ turbulence model has a lower error than *the* $k-\omega$. The simulation is suggested using 50000 elements because the error is not too far away from 100000 and needs a shorter time. All of this can be seen in Table 4.

This section discusses in-depth the ability of each turbulence model and cell meshing form to predict C_m. Figure 10(a) is C_m data for the S - A turbulence model with quadrilateral cells Mesh with 500 cells cannot follow the experimental C_m trend. On the other hand, the mesh with 5000, 50000, and 100000 cells showed similar results, especially at AoA≤11. After passing AoA=11°, the difference between the two is getting clearer. Meanwhile, compared with the results from experimental

Table 4 Average error percentages of all combinations of turbulence model and cell shape in predicting C_d

Turbulence model	Cells	Number of cells	Average error percentages 0°≤AoA≤ 9°
S-A	Quadrilateral	500	595.7725%
		5000	167.0722%
		50000	128.3462%
		100000	136.7055%
	Triangle	500	399.8685%
		5000	127.2159%
		50000	261.5862%
		100000	107.7466%
k-ε	Quadrilateral	500	553.8202%
		5000	164.3350%
		50000	127.7682%
		100000	110.4175%
	Triangle	500	349.5892%
		5000	120.4398%
		50000	72.5721%
		100000	101.4466%
k-ω	Quadrilateral	500	557.2969%
		5000	166.2224%
		50000	133.3429%
		100000	113.2809%
	Triangle	500	388.1673%
		5000	115.0269%
		50000	62.6635%
		100000	87.3908%

studies, both still show quite clear deviations. Mesh with 500 cells in this combination also does not follow the experimental C_m pattern. Meanwhile, for mesh with 50000 and 100000 cells, the results are identical in all AoA, as shown in Fig. 10(b). Figure 10(c) shows the computational results for the k - ε turbulence model for a mesh with quadrilateral cells with variations in the number of cells 500, 5000, and 50000. In more detail, it can be seen that before AoA=15°, the mesh with 50000 cells is closer to the experimental data when compared to a mesh with 5000 cells. On the other hand, at AoA=16° to AoA=24°, the mesh with 5000 cells shows better results than the mesh with cells 50000 cells. Although in the end, both of them could not show satisfactory results after AoA>11°. Both did not show a gradient change as in the experimental data. If the number of cells is increased to 100000, the results are similar to the simulation results using 50000 cells. However, at 17°≤AoA≤23°, there is a slight difference, although not too significant. Figure 10(d), the computational result for the $k - \varepsilon$ turbulence model with triangle cells shows slightly different results where the overall mesh with 5000 cells shows better results when compared to the computational results on the 50000 mesh. However, in extreme AoA, this combination cannot follow experimental results. Furthermore, the results obtained using a mesh of 100000 cells are even closer to 5000 cells than 50000 cells. Meanwhile, the computational results for the $k - \omega$ turbulence model with quadrilateral cells can be seen in Fig. 10(e). In Fig. 10(e), the conditions shown are similar to Fig. 10(c); however, there is a gradient change in the mesh with 500 cells. However, the changes also do not show better results. Figure 10(f), the computational result of the $k - \omega$ turbulence model with the triangle cells. The resulting trend is very similar to Fig. 10(d), where a mesh with 5000 cells gives a result closer to 100000 cells than a mesh of 50000 cells.

Table 5 shows the average error percentage for C_m. From the viewpoint of C_m, only the quadrilateral mesh with the k–ω turbulence model shows consistency. It can be seen from the decreasing error value as the number of cells increases. However, mesh with 50000 cells is recommended because the error value difference is 3.9087%, and the computation time is 29 minutes 14 seconds faster than 100000 cells.

If viewed as a whole from the mesh verification and validation of aerodynamic performances, it can be concluded that the best combination is the $k - \varepsilon$ turbulence model with 50000 quadrilateral cells within the asymptotic convergence range. Considering the accuracy of calculating the aerodynamic force coefficient of the airfoil, it is recommended to choose a quadrilateral mesh with 50000 or 100000 cells where the C_l errors of the two are similar. In addition, the quadrilateral mesh also shows consistency when predicting the C_d of the airfoil, even though the resulting error is not the smallest. Moreover, all combinations also show larger errors when calculating C_d than C_l. However, if the simulation is carried out to calculate the value of C_m, the quadrilateral mesh with the $k - \omega$ turbulence model is the best option because it shows consistency and errors that are not too big. In contrast, at 100000 cells, the error is only 18.1630%.

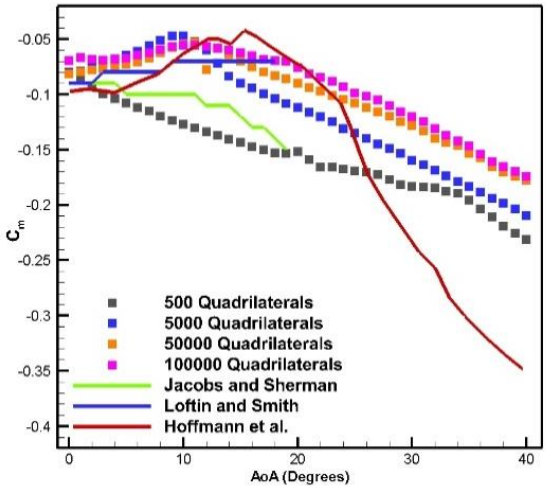

(a) S – A quadrilaterals

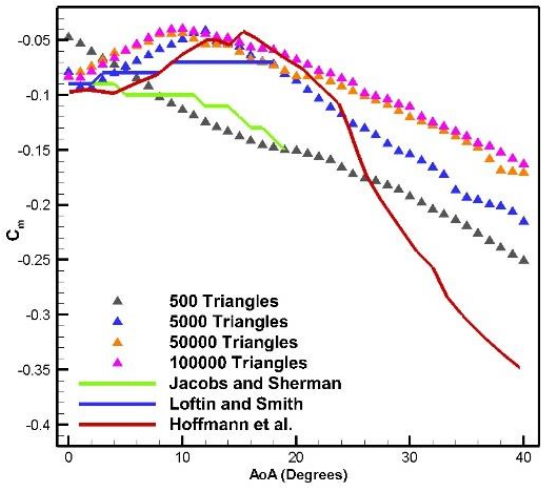

(b) S – A triangles

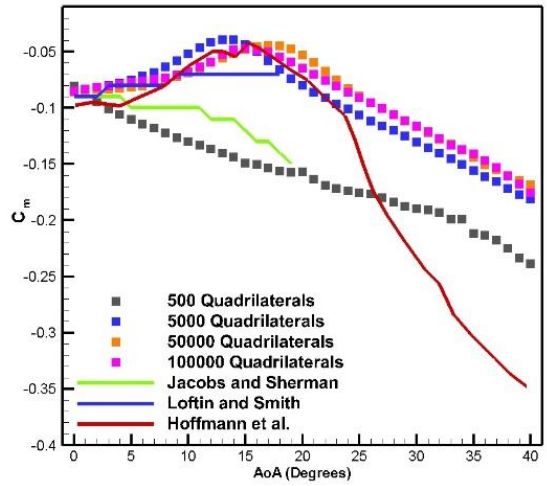

(c) k - ε quadrilaterals

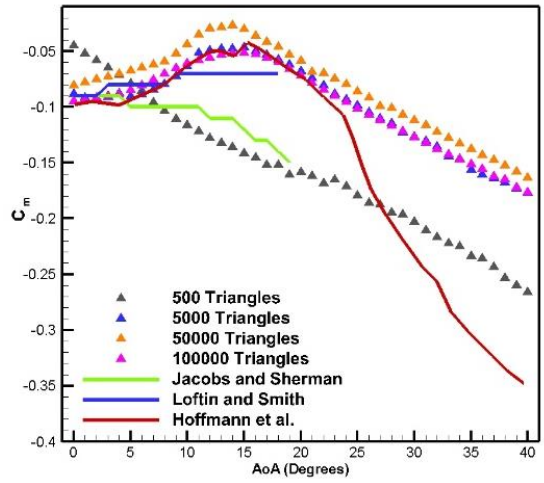

(d) k - ε triangles

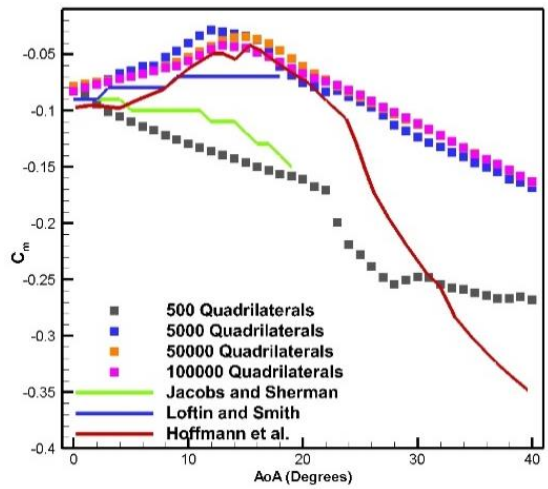

(e) $k-\omega$ quadrilaterals

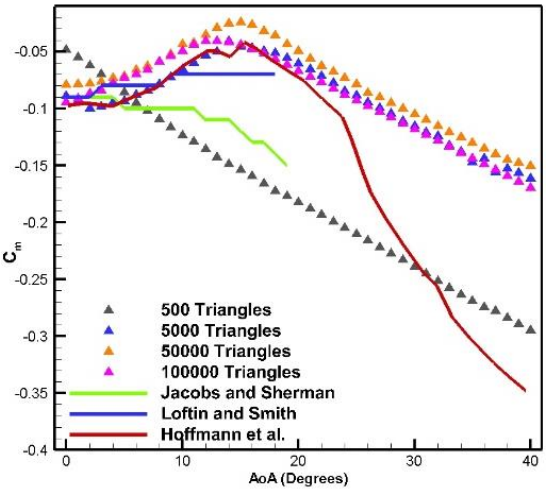

(f) $k-\omega$ triangles

Fig. 10 Plot C_m vs. AoA of each turbulence model and cell shape

The velocity contours for the S - A, k - ε, and k - ω turbulence models can be seen in Fig. 11. It can be seen that the S - A, k - ε, and k - ω turbulence models produce very identical velocity contours. The only visible difference is that the S - A turbulence model shows slightly more low-velocity areas in the tail of the airfoil. Figure 12 describes the pressure contours in each turbulence model. Here the pressure contours for the S - A, k - ε, and k - ω models are identical at the stagnation pressure location and in the area around the airfoil surface. Overall, all turbulence models show a pressure distribution on the upper side that is greater than the upper side so that the airfoil can produce a lift force. If the fluid flow is seen in a velocity streamline, it will look like in Fig. 13. The velocity streamlines results show no difference in S - A, k - ε, and k - ω turbulence models.

4. CONCLUSION

Overall, the results of this study conclude that the best combination of standard turbulence model, cell type, and the number of cells in modeling fluid flow at Reynolds number 10^6. Based on the results of the mesh refinement study, the quadrilateral mesh with the k–ε turbulence model shows that it is in the convergence range. If viewed from the accuracy in calculating the aerodynamic coefficient, several considerations must be considered. The mesh must be consistent. When the number of cells increases, the error value must be smaller. It is known that mesh with 50000 cells gives satisfactory results. The error

Table 5 Average error percentages of all combinations of turbulence model and cell shape in predicting C_m

Turbulence model	Cells	Number of cells	Average error percentages	
			0°≤AoA≤14°	15°≤AoA≤40°
S-A	Quadrilateral	500	65.0892%	66.4979%
		5000	28.8774%	43.1673%
		50000	20.5479%	38.8037%
		100000	22.0099%	36.0241%
	Triangle	500	234.9861%	236.9114%
		5000	15.7271%	28.2649%
		50000	19.9055%	37.7994%
		100000	26.6998%	36.3427%
k-ε	Quadrilateral	500	68.0050%	67.6707%
		5000	18.1313%	30.0010%
		50000	10.6387%	38.3377%
		100000	12.1374%	34.9563%
	Triangle	500	66.0237%	62.4707%
		5000	4.3785%	31.1847%
		50000	29.7877%	40.5288%
		100000	6.8310%	30.9840%
k-ω	Quadrilateral	500	67.5139%	68.1663%
		5000	31.2580%	33.8263%
		50000	22.0717%	39.3521%
		100000	18.1630%	35.7691%
	Triangle	500	71.5967%	71.6251%
		5000	4.3376%	36.4577%
		50000	27.2754%	47.4322%
		100000	17.7565%	33.7814%

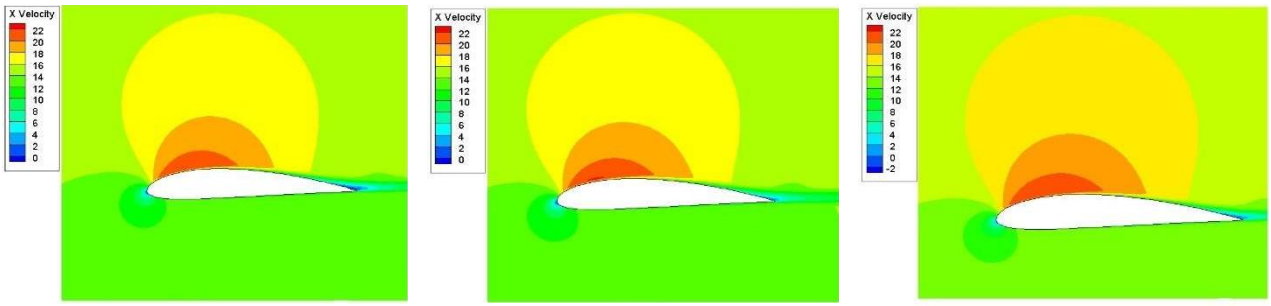

(a) S - A (b) k - ε (c) k - ω

Fig. 11 Velocity contour of each turbulence model

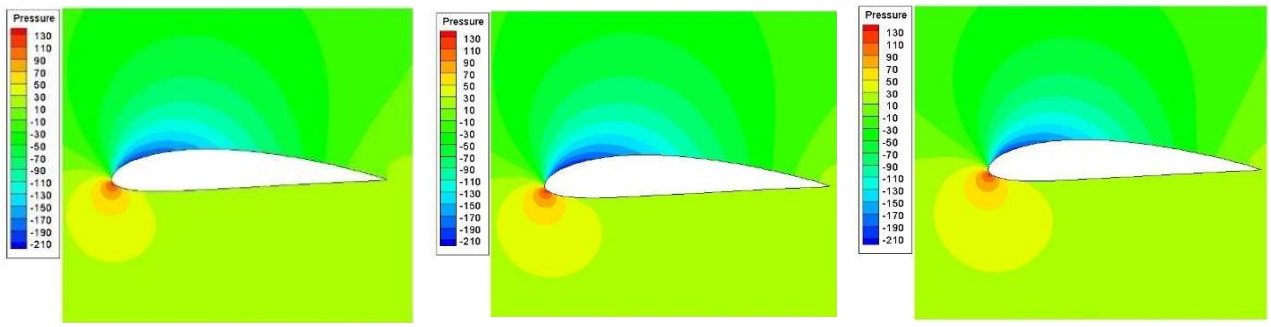

(a) S - A (b) k - ε (c) k - ω

Fig. 12 Pressure contour of each turbulence model

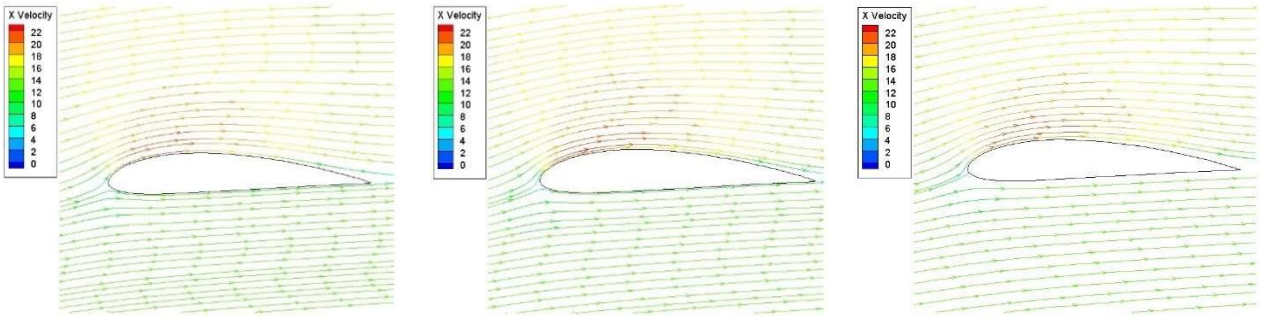

(a) S - A (b) k - ε (c) k - ω

Fig. 13 Pressure contour of each turbulence model

value in predicting c_l and c_d is 4.1151% and 128.7682%. although the error value of mesh with 50000 cells is bigger than 100000 cells, the computation difference benefits mesh with 50000 cells. the computation difference is 54 minutes. therefore, it is recommended to use mesh with 50000 cells. if considering c_m, the consistency is only shown in the quadrilaterals mesh with the k–ω turbulence mode. the error value for a mesh with 50000 cells is 22.0717%, and for 100000 cells, the resulting error value is 18.1630%. in contrast, the computation process of mesh with 50000 cells is 29 minutes and 14 seconds faster than mesh with 100000 cells.

REFERENCES

Aftab, S. M. A., Mohd Rafie, A. S., Razak, N. A., & Ahmad, K. A. (2016). Turbulence model selection for low Reynolds number flows. *PloS One*, *11*(4), e0153755. https://doi.org/10.1371/journal.pone.0153755

Ahadi, A., Sullivan, P. E., & Saghir, Z. (2018). *Comparison of Numerical and Experimental Results over a NACA0025 Airfoil Undergoing Separation*. https://doi.org/10.15406/fmrij.2018.02.00017

Ali, Z., Tucker, P. G., & Shahpar, S. (2017). Optimal mesh topology generation for CFD. *Computer Methods in Applied Mechanics and Engineering*, 317, 431-457. https://doi.org/10.1016/j.cma.2016.12.001

Anzalotta, C., Joshi, K., Fernandez, E., & Bhattacharya, S. (2020). Effect of forcing the tip-gap of a NACA0065 airfoil using plasma actuators: A proof-of-concept study. *Aerospace Science and Technology*, *107*. https://doi.org/10.1016/j.ast.2020.106268

Bhattacharya, S., & Ahmed, A. (2020). Effect of aspect ratio on the flow over a wall-mounted hemispherical turret. *International Journal of Heat and Fluid Flow*, 84. https://doi.org/10.1016/j.ijheatfluidflow.2020.108600

Bhattacharya, S., & Gregory, J. W. (2013). *The optimum wavelength of spanwise segmented plasma actuator forcing of a circular cylinder wake*. 51st AIAA Aerospace Sciences Meeting Including the New Horizons Forum and Aerospace Exposition 2013. https://doi.org/10.2514/6.2013-1011

Bouaziz, S., Deuss, M., Schwartzburg, Y., Weise, T., & Pauly, M. (2012). Shape-up: Shaping discrete geometry with projections. *Computer Graphics Forum*, 31(5), 1657–1667. https://doi.org/10.1111/j.1467-8659.2012.03171.x

Hills, J. L., Šafařík, P., & Sládek, A. (2005). Numerical modelling of turbulent flow past an airfoil. *Czech Technical University in Prague, Prague*.

Hoffmann, M. J., Reuss Ramsay, R., & Gregorek, G. M. (1996). *Effects of grit roughness and pitch oscillations on the NACA 4415 airfoil*. National Renewable Energy Lab.(NREL), Golden, CO (United States). https://doi.org/10.2172/266691

Hornshøj-Møller, S. D., Nielsen, P. D., Forooghi, P., & Abkar, M. (2021). Quantifying structural uncertainties in Reynolds-averaged Navier–Stokes simulations of wind turbine wakes. *Renewable Energy*, 164, 1550–1558. https://doi.org/10.1016/j.renene.2020.10.148

Iskandar, W., Julian, J., Wahyuni, F., Ferdyanto, F., Prabu, H. K., & Yulia, F. (2022). Study of airfoil characteristics on NACA 4415 with reynolds number variations. *International Review on Modelling and Simulations (IREMOS)*, 15(3), 162. https://doi.org/10.15866/iremos.v15i3.21684

Islam, M., Fürst, J., Wood, D., & Ani, F. N. (2016). Analysis of an airfoil using a transition and turbulence model. *Applied Mechanics and Materials*, 819, 356–360. https://doi.org/10.4028/www.scientific.net/AMM.819.356

Jacobs, E. N., & Sherman, A. (1937). Airfoil section characteristics as affected by variations of the Reynolds number. *NACA Technical Report*, 586, 227–267.

Jia, K., Scofield, T., Wei, M., & Bhattacharya, S. (2021). Vorticity transfer in a leading-edge vortex due to controlled spanwise bending. *Physical Review Fluids*, 6(2). https://doi.org/10.1103/PhysRevFluids.6.024703

Joshi, K., & Bhattacharya, S. (2019). Large-eddy simulation of the effect of distributed plasma forcing on the wake of a circular cylinder. *Computers and Fluids*, 193. https://doi.org/10.1016/j.compfluid.2019.104295

Julian, J., Iskandar, W., & Wahyuni, F. (2022a). Aerodynamics improvement of NACA 0015 by using Co-Flow jet. *International Journal of Marine Engineering Innovation and Research*, 7(4). https://doi.org/10.12962/j25481479.v7i4.14898

Julian, J., Iskandar, W., Wahyuni, F., & Ferdyanto, F. (2022b). Computational fluid dynamics analysis based on the fluid flow separation point on the upper side of the naca 0015 airfoil with the coefficient of friction. *Media Mesin: Majalah Teknik Mesin*, 23(2), 70–82. https://doi.org/10.23917/mesin.v23i2.18217

Julian, J., Iskandar, W., & Wahyuni, F. (2022c). Effect of single slat and double slat on aerodynamic performance of NACA 4415. *International Journal of Marine Engineering Innovation and Research* http://dx.doi.org/10.12962/j25481479.v7i2.12875

Julian, J., Iskandar, W., Wahyuni, F., & Bunga, N. T. (2022d). Characterization of the Co-Flow jet effect as one of the flow control devices. *Jurnal Asiimetrik: Jurnal Ilmiah Rekayasa & Inovasi*, 185–192. https://doi.org/10.35814/asiimetrik.v4i1.3437

Julian, J., Wahyuni, F., Iskandar, W., & Ramadhani, R. (2023a). The effect of curvature ratio towards the fluid flow characteristics in bend pipe based on numerical methods. *Turbo: Jurnal Program Studi Teknik Mesin*, 12(1). http://dx.doi.org/10.24127/trb.v12i1.2564

Julian, J., Iskandar, W., Wahyuni, F., & Nely Toding Bunga, dan. (2023b). Aerodynamic Performance Improvement on NACA 4415 Airfoil by Using Cavity. *Jurnal Asiimetrik: Jurnal Ilmiah Rekayasa Dan Inovasi*, *5*, 135–142. https://doi.org/10.35814/asiimetrik.v5i1.4259

Julian, J., Iskandar, W., & Wahyuni, F. (2023c). Leading edge modification of NACA 0015 and NACA 4415 inspired by beluga whale. *International Journal of Marine Engineering Innovation and Research*, 8(2). http://dx.doi.org/10.12962/j25481479.v8i2.16432

Kekina, P., & Suvanjumrat, C. (2017). *A comparative study on turbulence models for simulation of flow past NACA 0015 airfoil using OpenFOAM*. https://doi.org/10.1051/matecconf/20179512005

Khan, S. A., Bashir, M., Baig, M. A. A., & Ali, F. A. G. M. (2020). Comparing the effect of different turbulence models on the CFD predictions of NACA0018 airfoil aerodynamics. *CFD Letters*, 12(3), 1–10. https://doi.org/10.37934/cfdl.12.3.110OpenAccess

Kumar, B. R. (2019). Enhancing aerodynamic performance of NACA 4412 aircraft wing using leading edge modification. *Wind and Structures*, 29(4), 271–277. https://doi.org/10.12989/was.2019.29.4.271

Launder, B. E., & Spalding, D. B. (1983). The numerical computation of turbulent flows. *Numerical Prediction of Flow, Heat Transfer, Turbulence and Combustion*, 96–116. Elsevier. https://doi.org/10.1016/0045-7825(74)90029-2

Loftin Jr, L. K., & Poteat, M. I. (1948). *Aerodynamic characteristics of several NACA airfoil sections at seven Reynolds numbers from 0.7 x 10 (exp 6) to 9.0 x 10 (exp 6)*.

Panagiotou, C. F., Kassinos, S. C., & Aupoix, B. (2015). The ASBM-SA turbulence closure: Taking advantage of structure-based modeling in current engineering CFD codes. *International Journal of Heat and Fluid Flow*, 52, 111–128. https://doi.org/10.1016/j.ijheatfluidflow.2014.12.002

Reggio, M., Villalpando, F., & Ilinca, A. (2011). Assessment of turbulence models for flow simulation around a wind turbine airfoil. *Modelling and Simulation in Engineering*, 2011. https://doi.org/10.1155/2011/714146

Sadikin, A., Yunus, N. A. M., Abd Hamid, S. A., Salleh, S. M., Rahman, M. N. A., Mahzan, S., & Ayop, S. S. (2018). A comparative study of turbulence models on aerodynamics characteristics of a NACA0012 airfoil. *International Journal of Integrated Engineering*, 10(1). https://doi.org/10.30880/ijie.2018.10.01.019

Siddiqi, Z., & Lee, J. W. (2019). A computational fluid dynamics investigation of subsonic wing designs for unmanned aerial vehicle application. *Proceedings of the Institution of Mechanical Engineers, Part G: Journal of Aerospace Engineering*, 233(15), 5543–5552. https://doi.org/10.1177/0954410019852553

Sirignano, J., MacArt, J. F., & Freund, J. B. (2020). DPM: A deep learning PDE augmentation method with application to large-eddy simulation. *Journal of Computational Physics*, 423. https://doi.org/10.1016/j.jcp.2020.109811

Suvanjumrat, C. (2017). Comparison of turbulence models for flow past NACA0015 airfoil using OpenFOAM. *Engineering Journal*, 21(3), 207–221. https://doi.org/10.4186/ej.2017.21.3.207

Villalpando, F., Reggio, M., & Ilinca, A. (2011). Assessment of turbulence models for flow simulation around a wind turbine airfoil. *Modelling and Simulation in Engineering*, 2011, 1–8. https://doi.org/10.1155/2011/714146

Wilcox, D. C. (1998). *Turbulence modeling for CFD* (Vol. 2). DCW industries La Canada, CA.

Zhang, L., Gong, S., Lu, Z., Cheng, P., & Wang, E. N. (2022). Boiling crisis due to bubble interactions. *International Journal of Heat and Mass Transfer*, 182. https://doi.org/10.1016/j.ijheatmasstransfer.2021.121904